Hydrokinetic Resource Assessment in the Davao River: Integrating Flow Duration Curve with HEC-RAS 1D Model

Ken P. Cosares
Department of Civil Engineering, Ateneo de Davao University

Renyl B. Barroca
Department of Mechanical Engineering, Ateneo de Davao University

Vincent Noe L. Gimagan
Department of Civil Engineering, Ateneo de Davao University

Althea Alexa M. Bentayao
Department of Civil Engineering, Ateneo de Davao University

https://doi.org/10.5109/7395761

出版情報：Proceedings of International Exchange and Innovation Conference on Engineering & Sciences (IEICES). 11, pp.1889-1896, 2025-10-30. International Exchange and Innovation Conference on Engineering & Sciences
バージョン：

Hydrokinetic Resource Assessment in the Davao River: Integrating Flow Duration Curve with HEC-RAS 1D Model

Ken P. Cosares[1,3], Renyl B. Barroca[2,3], Vincent Noe L. Gimagan[1], Althea Alexa M. Bentayao[1]
[1]Department of Civil Engineering, Ateneo de Davao University
[2]Department of Mechanical Engineering, Ateneo de Davao University
[3]Center for Renewable Energy & Appropriate Technologies (CREATE), Ateneo de Davao University
Corresponding author email: kenpcosares@addu.edu.ph

Abstract: *This study conducted a hydrokinetic (velocity-based) resource assessment of the Davao River in Mindanao, Philippines. Using a twenty-year flow duration curve, nine steady-state flow boundary discharge rates were established within a calibrated 1D HEC-RAS model, discretized at 150-meter intervals. Depth-averaged velocities and channel depths were extracted to identify cross-sections that met the criteria of 1–2 m/s velocity and depths exceeding 1 meter for theoretical power density (PD) calculations. PD was estimated with the formula* $0.5\rho V^3 C_p$ *(where* $C_p = 1.0$ *for theoretical PD) and resulted in a reach-scale cumulative PD of 179.52 kW/m² at 10% exceedance probability, and 11.86 kW/m² at 90% exceedance probability. Potential sites are identified in the river segments situated along Barangays Callawa and Mandug. The identified sites are indicative of low-head turbine deployment but may necessitate higher-order modeling for a more robust hydrodynamic analysis. Nevertheless, the study's findings provide a foundational input for prototype design and techno-economic evaluations.*

Keywords: Hydrokinetic Resource Assessment; HEC-RAS; Power Density; Flow Duration Curve; Davao River

1. INTRODUCTION

Mindanao, locally recognized as the "fruit basket" of the Philippines and the nation's second largest island, exhibits a significant reliance on fossil fuel despite extensive river networks. As of 2023, coal accounts for approximately 61%` of the island's electricity generation, 30% from hydropower, and the remaining 9% from other renewables such as geothermal (4%), biomass (2%), solar (2%), and small power utilities (1%) [1]. Yet, the addition of new coal-based projects threatens to deepen this dependency unless the development of alternative renewable sources is prioritized. More than 80% of the Philippines' hydropower potential remains underdeveloped [2] and five of its highest-yielding provinces are in Mindanao, according to a national resource assessment report [3]. However, leveraging this resource requires methods that mitigate the social and ecological impacts associated with large dams [4], [5]. This raises critical questions regarding their net environmental benefits. Low-head hydrokinetic turbines present a viable alternative, as they generate electricity directly from in-stream velocity, have minimal civil works, and maintain the natural river morphology [6], [7], [8]. In the current study, a reach-scale hydrokinetic resource assessment for the Davao River is conducted in which a twenty-year discharge record was utilized, and a one-dimensional (1D) hydrodynamic modeling was implemented to identify potential sites, show their velocity fields, and quantify the theoretical power density for a given set of technical criteria. By shifting the assessment focus from potential energy (head-based) metrics to kinetic energy (velocity-based) measurements, this research aims to establish a baseline for further studies relating to hydrokinetic turbine design and optimization, techno-economic evaluation, socio-environmental impact study, among others, with the goal of progressing Mindanao's transition toward a cleaner energy future.

2. METHODOLOGY

Fig. 1 outlines the hydrokinetic resource assessment workflow adopted herein. Each process builds on the previous, beginning with the analysis of historical flow data to identify representative discharges as a function of exceedance probability, down to the calculation of theoretical power density – the primary assessment metric of this research.

2.1 Study Area

The study is focused on Davao River, situated on the island group of Mindanao in the Philippines. It is one of the largest rivers in the island and has significant potential for HK energy resource exploration due to its high flow characteristics [3]. The simulation domain is shown in Fig. 2. Specifically, the upstream portion begins in Lampianao, Calinan District, and the downstream ends in the estuary where the river meets the Davao Gulf, situated in the city center. The boundaries are selected in accordance with the limitations of the available digital elevation model (DEM).

2.2 Data Requirements

2.2.1 River Geometry Data

The high-resolution DEM data helps in modeling the river's bathymetry and terrain. It was used to extract the river cross-sections with the aid of the HEC-RAS built-in tool, the *RASMapper*. The DEM should have an appropriate resolution to accurately represent the river topography and bathymetry [9]. On the other hand, open-source web imagery (e.g. Open Street Maps and Google Satellite) was utilized to provide an accurate delineation of the riverbanks.

2.2.2 Hydrological Data

The 20-year monthly discharge records were sourced from the Department of Public Works and Highways (DPWH) – Region XI. The data were used to define the flow rate of the river as a function of "exceedance probabilities" or "chance of being equaled." A higher probability (say 90%) means that that certain flow is reached or exceeded 90% of the time, which translates to a low flow condition. On the other hand, a lower probability (say 10%) means a lower chance of achieving that flow rate. This occurs in conditions where the discharge is extremely high due to flash floods, typhoons, or other unusual hydrological events.

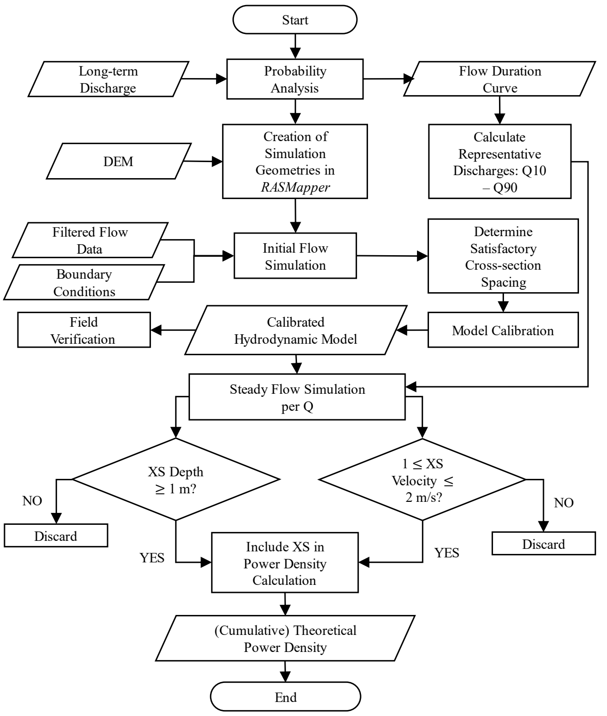

Fig. 1. Technical Workflow of the Hydrokinetic Resource Assessment

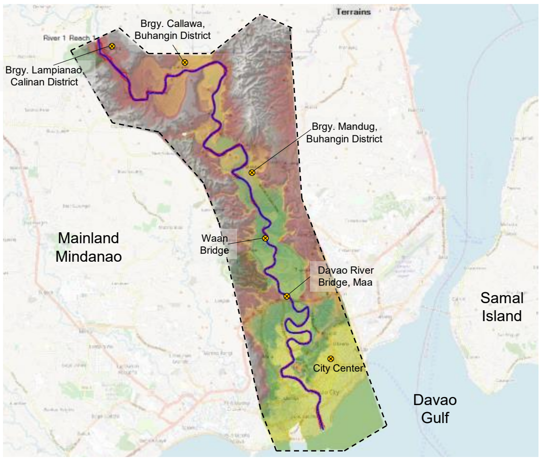

Fig. 2. Boundary Map of the Study Area

The long-term discharge data was pre-processed to generate the flow duration curve (FDC). After generating the FDC, representative discharges corresponding to 10% to 90% (Q10 – Q90) were interpolated and inputted into the HEC-RAS software to carry out the flow simulation.

The long-term water level data was used to supplement the discharge data, allowing calibration and validation of Manning's roughness coefficient. The data were requested from the Philippine Atmospheric, Geophysical, and Astronomical Services Administration (PAG-ASA) - Region XI. Literature suggests that the calibration of Manning's n requires either the analysis of bed material [10], field survey [10], comparison of observed and simulated water level [11], [12], [13] and estimation using secondary sources [10], [14], [15], [16].

2.3 Boundary Conditions

In this study, steady-state flow conditions are assumed. It means that flow characteristics such as discharge and velocity do not change over time. This was appropriate since the researchers are interested only in the distribution of the velocity magnitude for a specific period. Moreover, the generated FDC has already incorporated flow conditions over a long historical period. Additionally, the interest is not on the transient or rapidly changing events, such as in the case of flood-related studies. Under steady flow, the discharge remains constant along the river's length during the simulation. The velocity, depth profiles, and, subsequently, the power density are computed based on this steady discharge.

Furthermore, a one-dimensional (1D) numerical model was implemented similarly with relevant studies [17], [18], [19], [20] but of different objectives. In a 1D model, the flow is predominantly in the downstream direction, with lateral and vertical variations of flow being simplified. This is a reasonable assumption for long stretches of the river where variations in the flow patterns in the horizontal and vertical directions are minimal.

The upstream boundary condition defines how water enters the river system at the beginning of the modeled reach [15]. This condition was expressed as a normal depth corresponding to a specific discharge. The upstream discharge was varied and set to the flow corresponding to Q10 to Q90 obtained from FDC. The hydrodynamic properties for each of these flow conditions were observed to see how the velocity profile of the river is affected.

On the other hand, the downstream boundary condition tells how water exits the modeled river reach [15]. A common downstream boundary condition is the water surface elevation (WSE) at a known location, such as a gauging station near the mouth of the river. The WSE is used to calculate how the river discharges at this boundary and ensure that the hydraulic grade line is continuous throughout the reach. A normal depth boundary condition in the downstream is also common in HEC-RAS simulations [21], [22]. This assumes that the slope of the riverbed controls the outflow of water in the model. The slope can be estimated from the topographic data and can also be extracted from the DEM [22].

The flow regime in a river can be either subcritical, supercritical, or a combination of both (mixed). For this study, a mixed flow regime was assumed, although subcritical flow is common in high-volume rivers [23], [24].

Lastly, the initial selection of an appropriate Manning's n was based on the soil characteristics and land cover data. Moreover, secondary sources were used as starting points.

2.4 Model Setup, Calibration, and Verification

2.4.1 Model Setup

The acquired high-resolution DEM was imported in *RASMapper*. Cross-sectional profiles of the river channel were extracted from the DEM at appropriate intervals along the river's course. The initial estimate for the cross-section spacing (Δx) was based on the empirical formula suggested from the software's reference manual [15]:

$$\Delta x \leq \frac{0.15D}{S_0} \tag{1}$$

where D is the average main channel bankfull depth (feet), and S_0 is the bed slope (feet/feet). The selection of cross-section spacing requires a careful balance of accuracy and computational requirements. For example, a sufficiently dense model (as in Fig. 3a) can capture more detailed variations and potentially provide a more accurate representation of flow dynamics [25]. Therefore, modelers must consider the specific objectives of the study, the available computational resources, and the desired level of accuracy.

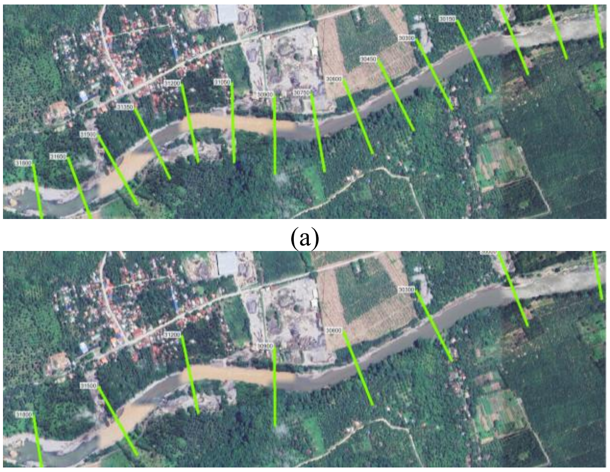

(a)

(b)

Fig. 3. Cross-sections Spaced at (a) 150 m, (b) 300 m (green line indicates cross-section of a 1D river model)

To determine the most appropriate cross-section spacing, a sensitivity analysis was conducted by setting up 11 different geometries, each with a unique cross-section spacing ranging from 1000 m down to 10 m. For each geometry, constant hydraulic parameters were applied. Model simulations were run for each geometry, and WSE was extracted at every cross-section. The change in WSE per unit spacing was then calculated and subsequently averaged. Finally, these average change values were plotted on an XY graph to visually identify the cross-section spacing at which the change in WSE per unit spacing demonstrated convergence.

2.4.2 Model Calibration

Following the determination of an appropriate cross-section spacing, the model was calibrated by iteratively adjusting Manning's n. This process involved running the model multiple times, each time comparing the simulated WSE at a designated control station to the observed WSE. The accuracy of the simulated results was quantitatively assessed using the root mean square of error (RMSE) over standard deviation (RSR) and Nash-Sutcliffe Efficiency (NSE), which are expressed as follows:

$$RSR = \frac{\sqrt{\sum_{i=1}^{N}\left(WSE_{i,obs} - WSE_{i,sim}\right)^2}}{\sqrt{\sum_{i=1}^{N}\left(WSE_{i,obs} - WSE_{ave,obs}\right)^2}} \tag{2}$$

$$NSE = 1 - \frac{\sum_{i=1}^{N}\left(WSE_{i,obs} - WSE_{i,sim}\right)^2}{\sum_{i=1}^{N}\left(WSE_{i,obs} - WSE_{ave,obs}\right)^2} \tag{3}$$

where N is the number of cross-sections, $WSE_{i,sim}$ and $WSE_{i,obs}$ are the simulated and observed water surface elevation at cross-section i, respectively. The goal of the calibration is to identify the n-value that gives the optimum RSR and NSE, thus yielding the best fit between the model and the observed data. Moreover, model performance was assessed and categorically described according to Table 1.

Table 1. Model's Performance Criteria [26], [27]

Performance Rating	RSR	NSE	PBIAS
Very Good	0-0.5	0.75	< $\pm$ 10
Good	0.5-0.6	0.65-0.75	$\pm$ 10 to $\pm$ 15
Acceptable	0.6-0.7	0.50-0.65	$\pm$ 15 to $\pm$ 25
Unsatisfactory	> 0.7	< 0.50	> $\pm$ 25

2.4.3 Model Verification

Once the model had been successfully calibrated, its predictive capability was assessed through field observation. This involves running the calibrated model for an independent time period (a period with observed data that was not used for calibration) and comparing the simulated results with the observed parameter at that period. A good agreement between the simulated and observed data during the verification period will confirm the model's reliability for simulating different flow scenarios. Percentage Bias (PBIAS) was used to evaluate the model's accuracy during the verification stage.

$$PBIAS = \frac{\sum\left(V_{i,sim} - V_{i,obs}\right)}{\sum\left(V_{i,obs}\right)} \times 100 \tag{4}$$

where $V_{i,sim}$ and $V_{i,obs}$ are the simulated and observed velocities, respectively. A positive PBIAS value indicates an underestimation of the velocities by the model, whereas a negative value suggests an overestimation. The magnitude of PBIAS determines the degree of deviation, which is categorized into performance ratings as outlined in Table 1.

2.4.4 Power Density Calculation

The power density (PD) is a metric that represents the power available per unit swept area of the turbine [18], and is calculated as:

$$PD = 0.5 \cdot \rho \cdot v^3 \cdot C_p \tag{5}$$

where ρ = 1000 kg/m^3, v is the average velocity at a specific cross-section, and C_p is a performance metric that accounts for the turbine's efficiency in converting the kinetic energy in flowing water into mechanical energy. The C_p factor was assumed at 1.0 within the scope of PD calculation but may actually vary depending on the site's hydraulic conditions and the hydropower's system design [28]. Consequently, the resulting PD values can be viewed as "theoretical" in nature. Further reductions of this theoretical PD are expected since all turbines do not operate at 100% efficiency. On the other hand, the water velocity and water depth derived from the model undergoes a filtering process prior to the computation of power density. This step is essential to ensure that only hydraulically viable locations for turbine deployment are considered [17]. Specifically, the technical criteria for inclusion are as follows: (1) average velocity must be between 1 – 2 m/s; (2) maximum main channel depth must be more than 1 m. These criteria consider the operational limitations of low-head turbines [29]. The cumulative power density was then calculated for each exceedance probability, which can be helpful for estimating the annual energy production (AEP) and a steppingstone for further studies.

3. RESULTS & DISCUSSION

3.1 Flow Duration Curve (FDC)

Fig. 4 illustrates the FDC derived from 198 monthly-average discharges measured between 2003 and 2024. This curve condenses 2 decades of hydrologic variability, with low exceedance percentages representing flood-dominated flows and high percentages indicating routine base-flow conditions.

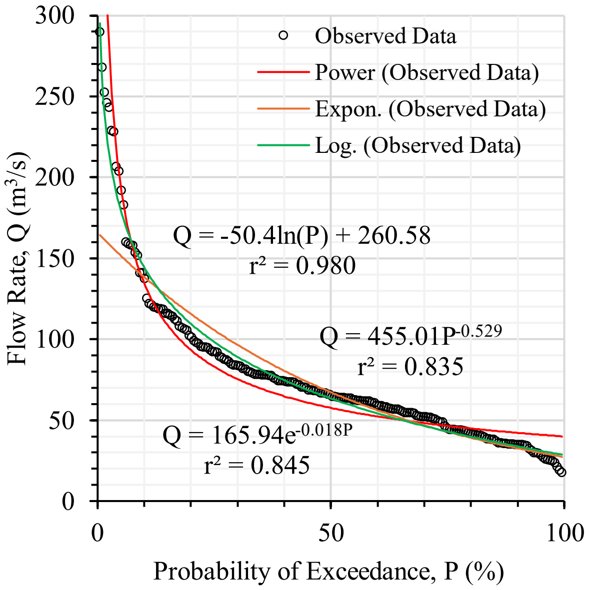

Fig. 4. Flow Duration Curve of Davao River (2003 – 2024)

Researchers attempted to fit power, logarithmic, and exponential expressions to the data. The logarithmic expression: $Q = -50.4 \ln P + 260.58$ yields the best fit with r^2 value of 0.980. The exponential function: $Q = 165.94e^{-0.018P}$ showed a relatively large deviation from the observed data, particularly at lower exceedance probabilities. The power function, on the other hand, gave the least, but still acceptable r^2 value of 0.835. The power and logarithmic functions both closely resembled the FDC scatter graph, with slight deviations at lower and higher exceedance probabilities. While conventionally, the highest r^2 values are preferred for fitting functions, visual inspection indicates that logarithmic expression provides the best overall representation of the data.

The logarithmic expression was used to calculate representative discharges shown in Table 2 and are used to encompass the full twenty-year hydrologic spectrum of the river. For example, the log-equation provides a Q10 of 144.52 m^3/s, indicating flash-flood conditions exceeded 10% of the time, and a Q90 of 33.79 m^3/s, reflecting the river's dry-season regime. A Q50 of 63.51 m^3/s illustrates the typical normal flow rate of the river. For conventional hydropower designs, a firm discharge corresponding to Q95 is recommended [30].

Table 2. Representative Q for the Flow Simulation

Flow Profile	Flow (m^3/s)	Flow Profile	Flow (m^3/s)	Flow Profile	Flow (m^3/s)
Q90	33.79	Q60	54.23	Q30	89.16
Q80	39.73	Q50	63.41	Q20	109.59
Q70	46.46	Q40	74.66	Q10	144.52

These discharges served as steady flow boundaries in the calibrated HEC-RAS model, ensuring that velocity outputs would reflect the long-term hydrological record rather than a single design event. This kind of approach also connects historical hydrology to reach-scale resource assessments, providing coherent flow scenarios for power density calculations and techno-economic evaluations. These representative flow values also capture the typical variability of the river, enabling precise analyses of potential hydrodynamic behaviors under different flow conditions [8].

3.2 Cross-section Spacing

The final 150-meter cross-section spacing was chosen to balance hydraulic accuracy and computational efficiency. Initial calculation using Equation (1) suggested a maximum spacing of 180 meters. Nevertheless, simulation outputs of the 11 geometries that were created and subjected under controlled conditions were compared, and the average change in water-surface elevation per unit spacing ($\Delta WSE/s$) is shown in Fig. 5.

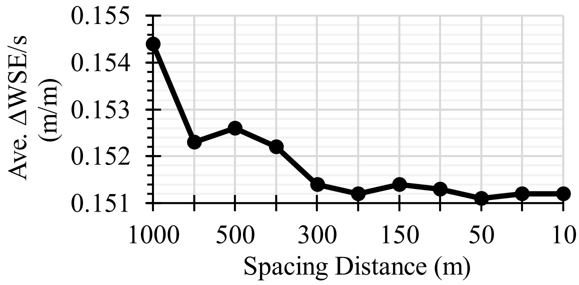

Fig. 5. Variation of $\Delta WSE/s$

The trend in Fig. 5 indicated that $\Delta WSE/s$ sharply decreased from 1000 m to 300 m, asymptotically approaching 0.151 m/m (approximately). Improvements from 100-m to denser spacing were less than 0.001 m/m, falling below the DEM's vertical resolution. Thus, spacing finer than 100 meters offered negligible benefits but could lead to complex computational handling (due to high volume of data) and software stability issues. This 150-meter spacing ensures stability while meeting the software Manual's criteria and provides adequate geometric resolution for identifying sub-reach scale power density hotspots without excessive computational cost.

3.3 Manning's n

Before the simulation proper, researchers calibrated the Manning's roughness coefficient (n) for the entire river reach to ensure accurate flow condition replication. Calibration focused on Station 11850, near the Maa Bridge, where the government's recording instruments are installed. This station served as the representative location for evaluating the model's performance. Table 3 shows the RMSE, RSR, and NSE values, which evaluate the agreement between observed and simulated WSE at this station. Among all values, Manning's n = 0.033 yields the optimal performance with r^2 value of 0.7346, as shown in Fig. 6.

Table 3. Model's Performance at Various Manning's n

n	RMSE	RSR	NSE
0.030	0.377	0.547	0.701
0.031	0.366	0.531	0.718
0.032	0.359	0.520	0.729
0.033	0.356	0.516	0.733
0.034	0.358	0.519	0.731
0.035	0.362	0.525	0.724
0.036	0.370	0.537	0.712

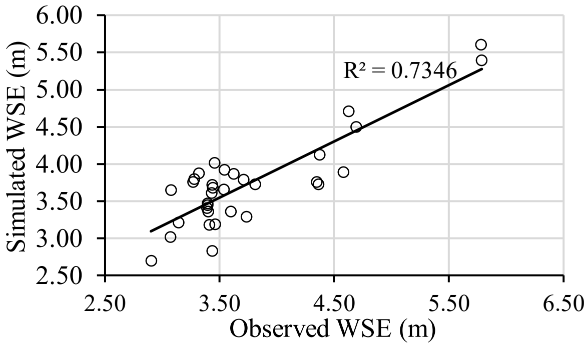

Fig. 6. Correlation between Observed and Simulated WSE at Station 11850 for n = 0.033

3.4 Field Verification

A field verification survey was conducted right after the model calibration. The primary parameters that were observed are the flow velocity and water depth. A stadia rod was used to measure depth, while a flow probe with an accuracy of ± 0.03 m/s was used to measure the velocity at varying depths. A GPS Data Logger was also utilized to record the position coordinates of each observation point.

Fig. 7. Field verification survey for computing independent discharge data. A stadia rod (left) and flow probe (right) were used to measure the depth and stream velocity, respectively.

While an equal spacing of points is generally recommended, the logistical challenges of navigating and traversing the river prevented a uniform distance between observation points. Despite this limitation, the data collected was sufficient for calculating an independent discharge. Each measurement took around 2 minutes, and the probe returns the time-averaged velocity at a specific depth of observation.

Using the velocity-area method, the total discharge at the time of observation was found to be 30.285 m^3/s. This discharge was then used as input for an independent flow simulation. After which, the corresponding velocity outputs were compared to the observed velocities at the time of observation. A PBIAS rating of -5.88% (see Table 4) indicates that the model slightly overestimated the observed velocities but remains accurate and reliable for river flow analysis.

Table 4. Analysis of Percentage Bias (PBIAS)

$\sum V_{i,obs}$	$\sum (V_{i,obs} - V_{i,sim})$	PBIAS (%)	Rating
3.4 m/s	-0.20 m/s	-5.88	Very Good

3.5 Velocity & Water Depth Plot

Fig. 8 and 9 show the spatial distribution of velocity at selected sites for Q90 and Q10, respectively. The velocity profile and the corresponding depth profile across the entire river are plotted in Fig. 10. There is a general decreasing trend from upstream to downstream, with upstream sections experiencing sharp fluctuations due to local channel features, while downstream sections exhibit more stable and lower speeds. Velocity behavior also varied with exceedance probabilities – higher velocities have lower probability of being exceeded since they only occur during high-flow hydrological events. On the other hand, lower velocities were observed under more certain conditions. The analysis further revealed that there is a general inverse relationship between depth and velocity (as shown in Fig. 10), where higher velocities are often observed in shallower areas and slow velocities in deeper zones. While this trend holds in most sections, some midstream areas show weaker correlations and exceptions, underscoring variability in flow behavior. Understanding these patterns is crucial for identifying optimal sites for hydrokinetic energy deployment, where both sufficient velocity and depth are needed for effective and safe turbine installation.

3.6 Potential Sites

To assess the hydrokinetic energy potential of the river, specific areas were selected based on the overall velocity profile and the corresponding water depth. Site selection was guided by criteria that ensure both technical feasibility and operational safety. Key among these was the velocity range between 1 m/s and 2 m/s – meeting the minimum cut-in speed required for most hydrokinetic turbines and avoiding performance issues such as cavitation and mechanical stress that may occur above 2 m/s [31]. Optimal turbine performance is often achieved between 1.5 – 3.5 m/s , with peak efficiency around 2 m/s [31]. The threshold of 2 m/s [29], as represented by yellow to red colors in the contour map (see Fig. 8, 9), can be used to visually identify suitable high velocity zones.

In hydrokinetic turbines, operating outside the optimal velocity range can lead to inefficient flow patterns around the blades, reducing energy capture and potentially increasing wear. These losses are especially crucial in shallow flows or when the velocity is too low to maintain streamlined conditions. Therefore, maintaining a target

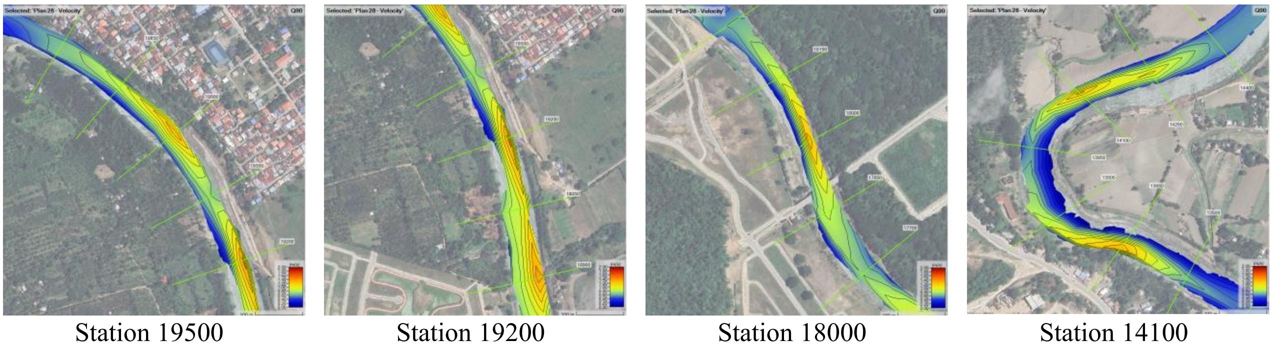

Fig. 8. Velocity Contour Map of Selected Sites at Q90 = 33.79 m^3/s

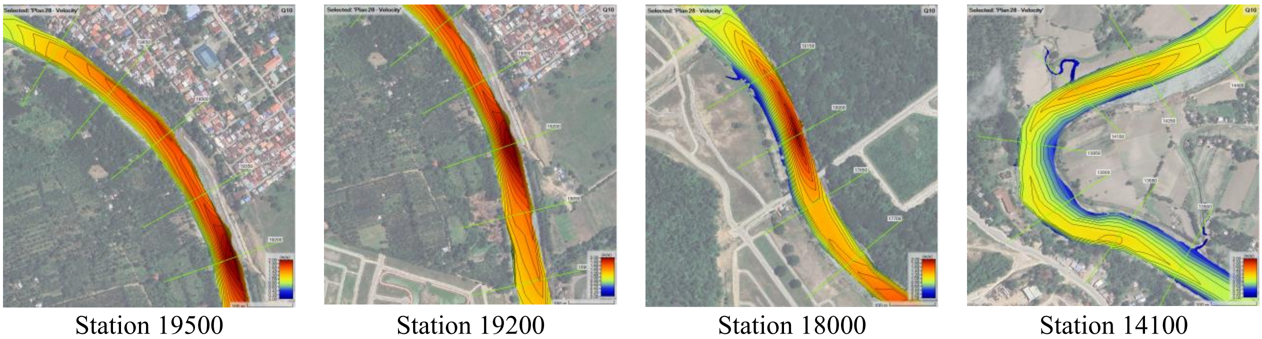

Fig. 9. Velocity Contour Map of Selected Sites at Q10 = 144.52 m^3/s

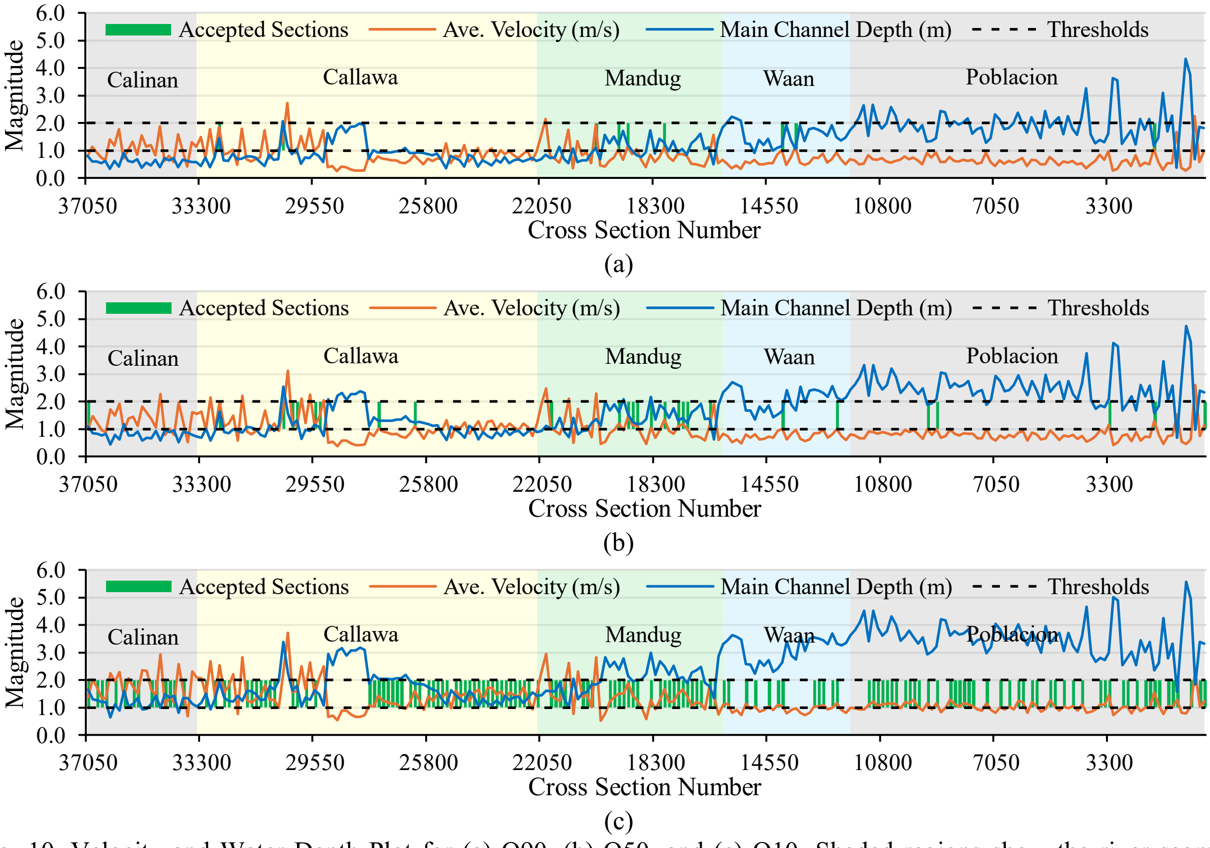

Fig. 10. Velocity and Water Depth Plot for (a) Q90, (b) Q50, and (c) Q10. Shaded regions show the river segment bounded by the indicated barangay.

velocity between 1 – 2 m/s and ensuring a minimum depth of 1 meter helps minimize such losses, supporting both performance and longevity.

The green-shaded areas in Fig. 10 indicate sections meeting the criteria. Upstream sections (Calinan) often show sufficient velocity but insufficient depth, while downstream areas (Poblacion) have greater depth but generally lack the required velocity at median flows. As exceedance probability increases from 10% to 90%, the number of acceptable sections decreases, reflecting reduced suitability for turbine installation during lower flow conditions. However, a number of cross-sections in the vicinity of Barangay Callawa, Mandug, and Waan consistently meet both criteria across all exceedance levels, which indicates stable and favorable hydraulic conditions that make them promising spots for hydrokinetic energy deployment.

Table 5. Cross-sections that consistently satisfy velocity and depth criteria from Q10 to Q90

Station Number	Velocity Range (m/s)	Depth Range (m)	Location
19500	1.04 – 1.5	1.20 – 2.37	Mandug
19200	1.14 – 1.88	1.22 – 2.15	Mandug
18000	1.09 – 1.67	1.31 – 2.49	Mandug
14100	1.00 – 1.05	1.15 – 2.64	Waan
1800	1.06 – 1.54	1.18 – 2.36	Poblacion

Table 5 shows the river cross-sections that consistently meet the required velocity and depth thresholds across all modeled flow conditions. This consistent compliance suggests a strong potential for sustained hydrokinetic energy generation regardless of flow variability. Notably, the cross-section at station 19200, near Mandug Bridge, demonstrated the highest and most stable velocity values —from 1.88 m/s at Q10 to 1.14 m/s at Q90– while maintaining a minimum depth of 1.22 m. These reliable hydraulic characteristics position the area as one promising site for hydrokinetic energy deployment. Overall, the consistently favorable conditions at these identified sites support their suitability for long-term and efficient hydrokinetic energy system installation.

3.7 Power Density

For each representative discharge, the theoretical power density was calculated for each accepted cross-sections using Equation (5), and then these values were summed along the entire river to derive a cumulative theoretical power density. The results are presented in Fig. 11, which shows a noticeable decline from 179.52 kW/m^2 at Q10 to 11.86 kW/m^2 at Q90. A significant portion of this decrease occurs between Q10 and Q40, where the overall resource diminishes by nearly 77%. Beyond Q60, the curve flattens, and the difference between Q70, Q80 and Q90's PD became minimal. Further reductions were observed once the depth-averaged velocity fell below 1.2 m/s.

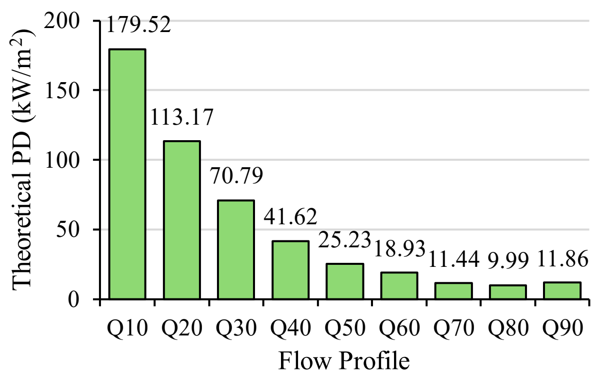

Fig. 11. Theoretical Power Density of Davao River Considering Velocity & Depth Criteria for Hydrokinetic Deployment

The velocity and depth plots in Fig. 10 indicate that two barangays – Callawa and Mandug—are responsible for supplying most of the river's usable energy. For example, during the rare Q10 high-flow event, Callawa alone accounts for nearly 40% of the total PD, attributed to its deep, narrow pools that maintain fast-moving, well-submerged water. Mandug contributes roughly 22% of the total energy, due to several fast-flowing riffle-pool sections. Poblacion provides around 19%, benefiting from consistent depths even though its water speed rarely exceeds 1.2 m/s, but it is densely populated by urban developments. As flow rates decline toward normal levels (high exceedance percentages), many shallow upstream sections fail to meet the velocity + depth criteria; however, these 2 barangays continue to do so. At median flow (Q50), roughly 80% of the total resource comes from these segments, and is sufficient to power small turbine arrays for most of the year. Although the river's energy potential diminishes as water velocity slows, river segments within the 2 cited areas remain a dependable location that may become a compelling starting point for future techno-economic evaluations.

4. CONCLUSION

A steady flow one-dimensional HEC-RAS model has been calibrated using two decades of discharge data and discretized at 150-meter cross-section intervals. The model yielded a hydraulically consistent representation of a specific reach of the Davao River Basin where hydrokinetic resource assessment can be implemented. By employing turbine-specific thresholds for both velocity and depth, the model facilitated the simulation of a long-term flow variability leading to reach-scale power density estimates at a certain exceedance probability. Finally, potential sites that were technically viable for hydrokinetic deployment were identified. Independent field measurements at the Waan Bridge confirmed the model's reliability and showed a minimal bias between observed and simulated discharges. The numerical and field results collectively provide a validated river model, but a higher degree of modeling is recommended for a more robust resource assessment. Nevertheless, the results of this study can be utilized to estimate annual energy production, size prototype turbines, and assess the techno-economic feasibility of low-head hydrokinetic systems for future studies.

5. REFERENCES

[1] "2023 Power Statistics: Department of Energy—Philippines." Accessed: Nov. 15, 2024. [Online]. Available: https://legacy.doe.gov.ph/energy-statistics/2023-power-statistics

[2] "Philippines: Country Profile | Hydropower & Dams International." Accessed: Nov. 15, 2024. [Online]. Available: https://www.hydropower-dams.com/news/philippines-country-report/

[3] M. R. C. Ang et al., "Philippine Renewable Energy Resource Mapping from LiDAR Surveys (REMap): Terminal Report," University of the Philippines Diliman, Terminal Report, 2017.

[4] A. Kumar et al., "Hydropower — IPCC." Accessed: Nov. 09, 2024. [Online]. Available: https://www.ipcc.ch/report/renewable-energy-sources-and-climate-change-mitigation/hydropower/

[5] L. Berga, "The Role of Hydropower in Climate Change Mitigation and Adaptation: A Review," Engineering, vol. 2, no. 3, pp. 313–318, Sep. 2016, doi: 10.1016/J.ENG.2016.03.004.

[6] B. Kirke, "Hydrokinetic turbines for moderate sized rivers," Energy for Sustainable Development, vol. 58, pp. 182–195, Oct. 2020, doi: 10.1016/j.esd.2020.08.003.

[7] M. Sood and S. K. Singal, “Development of hydrokinetic energy technology: A review,” International Journal of Energy Research, vol. 43, no. 11, pp. 5552–5571, 2019, doi: 10.1002/er.4529.
[8] W. I. Ibrahim, M. R. Mohamed, R. M. T. R. Ismail, P. K. Leung, W. W. Xing, and A. A. Shah, “Hydrokinetic energy harnessing technologies: A review,” Energy Reports, vol. 7, pp. 2021–2042, Nov. 2021, doi: 10.1016/j.egyr.2021.04.003.
[9] S. Saksena and V. Merwade, “Incorporating the effect of DEM resolution and accuracy for improved flood inundation mapping,” Journal of Hydrology, vol. 530, pp. 180–194, Nov. 2015, doi: 10.1016/j.jhydrol.2015.09.069.
[10] W. L. Cowan, “Estimating hydraulic roughness coefficients,” Agricultural engineering, vol. 37, no. 7, pp. 473–475, 1956.
[11] S. A. Abbas, A. H. Al-Aboodi, and H. T. Ibrahim, “Identification of Manning’s Coefficient Using HEC-RAS Model: Upstream Al-Amarah Barrage,” Journal of Engineering, vol. 2020, no. 1, p. 6450825, 2020, doi: 10.1155/2020/6450825.
[12] P. K. Parhi, “HEC-RAS Model for Mannnig’s Roughness: A Case Study,” vol. 2013, Jul. 2013, doi: 10.4236/ojmh.2013.33013.
[13] Mohd Aliff Mohd Anuar, Mohd Shalahuddin Mohd Adnan, Lim Foo Hoat, Veianthan Jayaramu, Lee Wei Koon, and Mohamad Hafiz Hassan, “Evaluating Calibration Potential in River Hydraulic Modelling Based on Critical Slope: A Case Study of Sungai Pahang Basin,” Proceedings of International Exchange and Innovation Conference on Engineering & Sciences (IEICES), vol. 10, pp. 602–608, Oct. 2024, doi: 10.5109/7323323.
[14] W. F. Coon, Estimation of roughness coefficients for natural stream channels with vegetated banks. in U.S. Geological Survey water-supply paper, no. 2441. Denver, CO: U.S. Geological Survey, 1998.
[15] G. Brunner, HEC-RAS Hydraulic Reference Manual. in Version 6.7_Beta. 2025.
[16] “Guide for selecting Manning’s roughness coefficients for natural channels and flood plains,” 1989. doi: 10.3133/wsp2339.
[17] P. Jacobson, “Assessment and Mapping of the Riverine Hydrokinetic Resource in the Continental United States,” Dec. 2012, doi: 10.2172/1219876.
[18] M. T. Tigabu, D. H. Wood, and B. T. Admasu, “Resource assessment for hydro-kinetic turbines in Ethiopian rivers and irrigation canals,” Energy for Sustainable Development, vol. 58, pp. 209–224, Oct. 2020, doi: 10.1016/j.esd.2020.08.005.
[19] P. Punys, I. Adamonyte, A. Kvaraciejus, E. Martinaitis, G. Vyčienė, and E. Kasiulis, “Riverine hydrokinetic resource assessment. A case study of a lowland river in Lithuania,” Renewable & Sustainable Energy Reviews, vol. 50, pp. 643–652, Oct. 2015, doi: 10.1016/j.rser.2015.04.155.
[20] R. D. Montoya Ramírez, F. I. Cuervo, and C. A. Monsalve Rico, “Technical and financial valuation of hydrokinetic power in the discharge channels of large hydropower plants in Colombia: A case study,” Renewable Energy, vol. 99, pp. 136–147, Dec. 2016, doi: 10.1016/j.renene.2016.06.047.
[21] T. P. Suro, M. J. Niemoczynski, and A. Boetsma, “Development and calibration of HEC–RAS hydraulic, temperature, and nutrient models for the Mohawk River, New York,” U.S. Geological Survey, 2024–5005, 2024. doi: 10.3133/sir20245005.
[22] M. Beza, A. Fikre, and A. Moshe, “Dam Breach Modeling and Downstream Flood Inundation Mapping Using HEC-RAS Model on the Proposed Gumara Dam, Ethiopia,” Advances in Civil Engineering, vol. 2023, no. 1, p. 8864328, 2023, doi: 10.1155/2023/8864328.
[23] M. Paoletti et al., “Discharge Monitoring in Open-Channels: An Operational Rating Curve Management Tool,” Sensors, vol. 23, no. 4, Art. no. 4, Jan. 2023, doi: 10.3390/s23042035.
[24] A. Mobasher and A. Mahmoud, “Backwater Rise Due to Bridge Piers in Curved Channels under Subcritical Flow Conditions,” Aust. J. Basic & Appl. Sci., vol. 13(1), pp. 117–127, Jan. 2019, doi: 10.22587/ajbas.2019.13.1.15.
[25] P. Brue, “How to Draw HEC-RAS Cross Sections,” Paige Brue. Accessed: Oct. 04, 2024. [Online]. Available: https://www.paigebrue.com/how-to-draw-hec-ras-cross-sections/
[26] D. N. Moriasi, J. G. Arnold, M. W. Van Liew, R. L. Bingner, R. D. Harmel, and T. L. Veith, “Model Evaluation Guidelines for Systematic Quantification of Accuracy in Watershed Simulations,” Transactions of the ASABE, vol. 50, no. 3, pp. 885–900, 2007, doi: 10.13031/2013.23153.
[27] S. Shrestha, M. Shrestha, and P. K. Shrestha, “Evaluation of the SWAT model performance for simulating river discharge in the Himalayan and tropical basins of Asia,” Hydrology Research, vol. 49, no. 3, pp. 846–860, Apr. 2017, doi: 10.2166/nh.2017.189.
[28] Md. Z. Alam and Y. Watanabe, “Efficiency calculation of hydro turbine in varying head condition and its effect on system design,” in Proceedings of International Exchange and Innovation Conference on Engineering & Sciences (IEICES), Kyushu University, Japan: Interdisciplinary Graduate School of Engineering Sciences, Kyushu University, Oct. 2017, pp. 7–9. doi: 10.15017/1906116.
[29] B. Kirke, “Towards more cost-effective river hydrokinetic turbines,” Energy for Sustainable Development, vol. 78, p. 101370, Feb. 2024, doi: 10.1016/j.esd.2023.101370.
[30] Guideline and Manual for Hydropower Development Vol. 2 Small Scale Hydropower, Mar. 2011. [Online]. Available: https://openjicareport.jica.go.jp/pdf/12024899.pdf
[31] J. B. Johnson and D. J. Pride, “River, Tidal, and Ocean Current Hydrokinetic Energy Technologies: Status and Future Opportunities in Alaska,” Alaska Center for Energy and Power, Alaska, USA, Nov. 2010. [Online]. Available: https://aippa.info/wp-content/uploads/2012/03/2010_11_1_State_of_the_Art_Hydrokinetic_Final.pdf